ECCOMAS Congress 2016
VII European Congress on Computational Methods in Applied Sciences and Engineering
M. Papadrakakis, V. Papadopoulos, G. Stefanou, V. Plevris (eds.)
Crete Island, Greece, 5–10 June 2016

LARGE-EDDY SIMULATION AND FAR FIELD ACOUSTICS OF A SUBSONIC HOT JET

O. Labbé

ONERA - The French Aerospace Lab
F-92322 Châtillon, France
odile.labbe@onera.fr

Keywords: LES, Hot Turbulent Jet, Ffowcs Williams and Hawkings.

Abstract. *The present work deals with the numerical simulation of a hot subsonic turbulent jet using LES. The main difficulty is to obtain a turbulent jet flow right from the exhaust of the nozzle, as in real jets for Reynolds numbers over 10^5. Injecting disturbances in the boundary layer inside the nozzle to force the transition from a laminar state to a turbulent one, may introduce spurious noise which can pollute the acoustic field. Experimental measurements on mean velocity and near and far field pressure were carried out in the Onera CEPRA19 anechoic wind tunnel on a nozzle of diameter D= 80 mm, called Φ80. These measurements constitute a database to validate numerical simulations. The aerodynamic solver is based on the compressible Navier–Stokes equations expressed in conservative form with a spatial discretization method based on the cell-centered Finite Volume methodology on structured grid. The influence of mesh refinement is studied, thanks to a comparison between a fine and very fine mesh including respectively 30 and 240 millions elements on the same jet configuration. The noise radiation is performed using the Ffowcs Williams and Hawkings surface formulation, that computes time pressure histories at any observer location by integration of the flow field solution on a control surface surrounding the jet and containing all the noise sources. The near and far fields are compared to experimental measurements. Discrepancies remain close to the nozzle exit which lead to an overestimation of the pressure levels in both near and far fields, especially near the 90◦ angular sector.*

1 INTRODUCTION

With the increase of computational capacities in the last decades, it became possible to perform unsteady flow simulations to reproduce and investigate noise generation [1]. If direct numerical simulations (DNS) are still limited to the simulation of low Reynolds, academic configurations [2][3], the use of large-eddy simulations (LES) allows to compute higher Reynolds number, turbulent flows [4]-[8] more representative of the industrial concerns. However, performing a Large Eddy Simulation (LES) of a turbulent jet able to reproduce the experimental behavior is still a challenge despite the progresses made over the recent years. One of the difficulties is to obtain a turbulent jet flow right from the exhaust of the nozzle, as in real jets [9] for Reynolds numbers over 10^5. A very fine resolution of the boundary layers inside the nozzle is then necessary, which leads to prohibitive computational resources for experimental boundary layers thickness. So, the numerical jets tend to be laminar at the nozzle exit and as a consequence, strong vortex pairings appear in the shear layer, what usually does not occur in the experiments at higher Reynolds numbers. An additional noise source is then observed in the numerical far-field pressure spectra in the medium frequencies when compared to the measured ones [10]-[13]. Downstream of the laminar part of the flow, the transition towards the turbulent regime is then abrupt, as seen through shear layer properties (faster spreading rate), leading to an underestimation of the potential core length. A key issue of the success of such simulations is to provide boundary conditions representative of the anechoic facilities where jet noise experiments are performed. Several approaches have been developed to allow the turbulent transition of the jets. It is a difficult problem because the jet forcing must generate a minimum spurious noise, in order to avoid to contaminate the acoustic field. The jet development is strongly linked to the initial turbulent or laminar shear layer state, as observed by Zaman [9], the latter leading to additional noise. Non-reflecting conditions are required at lateral and outflow boundaries to model the free-field conditions and to avoid spurious noise contamination of the physical sound field [14]. For a detailed review of available numerical boundary conditions for aeroacoustic simulations, the reader may refer to Tam [15].

Several authors such as Ukeiley and Ponton [16], Suzuki and Colonius [17], Muller *et al.* [19], Fayard *et al.* [20], or Hall *et al.* [21] highlighted the importance of the low order azimuthal modes particularly for position close to the potential core end. Previously, Lorteau *et al.* [22] performed an analysis of the near field pressure from an experimental database of an isothermal and a hot subsonic jet. They established the existence of a sector linked to an acoustic behaviour in the near field in which the low frequencies around St = 0.2 and the axisymmetric mode are dominant.

In the present work, a numerical simulation using the LES methodology is carried out on a hot subsonic jet in order to analyze its near pressure field and its links to the jet flow and to the acoustic far field. The influence of mesh resolution on jet flow development and noise radiation is investigated using LES combined with the Ffowcs Williams & Hawkings surface integral formulation [23] to simulate the far-field noise. No turbulence seeding is made in the boundary layers. Several experimental [19][24] and numerical investigations [10][18]-[20][22][25][26] in the past were carried out on this jet configuration and experimental data are available for comparison with simulation results. The paper is organized as follows. Details of the simulated configuration are given in section 2, where the geometric configuration, numerical parameters for flow and noise simulations and the computational grids are also described. Unsteady and steady flow fields and radiated noise are then presented in Section 3 through comparison with experimental data acquired on the same jet configuration. Mean flow and turbulence evolutions are especially detailed upstream and downstream of the nozzle. Several effects of the meshing on the aerodynamic and acoustic fields are also presented in

this section. Near and far fields are analyzed and different control surfaces are used for the FW-H formulation and compared.

2 JET CONFIGURATION

The geometry considered is a round nozzle with an exhaust diameter D of 80 mm. The jet static temperature is T_j = 830 K and its Mach number is M_j = 0.7, which corresponds to a jet velocity U_j of 410 m/s. The Reynolds number based on nozzle diameter is $Re_D = U_j D/\nu = 4 \times 10^5$, where ν for the kinematic viscosity. The ambient pressure and temperature are p_0 = 101,325 Pa and T_0 = 280 K, respectively. Aerodynamic and acoustic measurements, performed in the CEPRA19 anechoic facility of Onera [19] [24] are available for comparisons with simulations. The characteristics of this single jet are provided in Table 1. They lead to a Reynolds number of 400,000 based on the nozzle diameter and the jet velocity. Because of the high temperature of the jet, the jet velocity U_j at the nozzle exit is lower than the local sound velocity c_j but higher than the sound velocity c_∞ outside the jet. So, the local Mach number $M_j=U_j/c_j$ is subsonic whereas the convective Mach number $M_c=(U_j+c_j)/(c_j+c_\infty)$ is supersonic. The following table summarizes the jet characteristics with subscripts j, tot and ∞, respectively, representing jet exit conditions, jet total stagnation characteristics and ambient conditions.

U_j (m.s−1)	M_j	T_j/T_∞	U_j/c_∞	T_{tot}/T_∞	T_∞ (K)	Re_D	p_{tot}/p_∞
410	0.7	2.96	1.2	3.2	280	4×10^5	1.4

Table 1: jet characteristics with subscripts j, tot and ∞, respectively, representing jet exit conditions, jet total stagnation characteristics and ambient conditions.

The computational domain is cylindrical and extends from X/D = -29 to 100 and has a radius of 80D. An illustration of the nozzle with a detail of the nozzle exit is given in Figure 1. Inside the nozzle, the inflow condition is located 7.15 diameters upstream of the exhaust. A first contraction is present for -6 < X/D < -5.5, followed by a slowly converging shape up to the nozzle exit where a second contraction is visible (-0.16 X/D). The nozzle fairing starts with a radius of 2.5 diameters at X/D =-29 to -18.5 and converges up to X/D = -13 with an angle of 4.3◦ and then up to X/D = -0.5 with an angle of 6.9° . At the exhaust, an angle of 16.4° is visible.

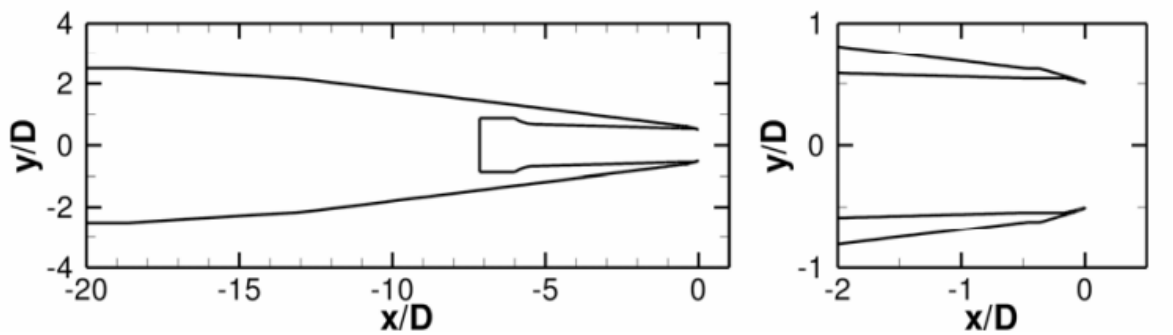

Figure 1: Illustrations of the nozzle shape.

2.1 Grid parameters

Two meshes have been used in this study. The first one called 'Fine' is issued from Huet [10] and consists in $30x10^6$ cells, while the second one called 'Very Fine' contains 240 $x10^6$

cells and was provided by Lorteau *et al.* [22]. The grid of both meshes is axi-symmetrical and structured and includes a O-type treatment on the jet axis to ensure that hexahedral cells have an homogeneous size in the core region. A refined zone which extends downstream of the nozzle exit from (X/D = 0 ; r/D = 2) to (X/D = 25 ; r/D = 5) and upstream of the nozzle exit up to (X/D = -2 ; r/D = 2.4) has been imposed for a good resolution of the jet flow development. Bogey *et al.* [12] tested different azimuthal discretizations and showed the importance of this grid parameter on the shear layer development and jet properties: the 'Very Fine' grid has four times more cells (480) in the azimuthal direction than the 'Fine' grid (120). The grid is stretched from a refined zone, in which the flow is accurately calculated, to the simulated domain boundaries in order to damp acoustic waves before they reach the borders and thus avoid spurious reflections. The details of mesh refinement can be found in the respective papers [10] [22]. The main characteristics of both grids are summarized in Table 2.

Grid name	$\Delta x/D$ (%)	$\Delta r_j/D$ (%)	$r_j.\Delta\theta/D$(%)	St_{cut}	Number of Cells$\times 10^6$	$T.U_j/D$
Fine	0.25	0.25	2.6	0.5	30	512
Very Fine	0.06	0.03	0.6	1	240	449

Table 2: Characteristics of both grids, $\Delta x/D$ and $\Delta r_j/D$ at X/D = 0 and $r_j.\Delta\theta/D$ at r_j = D /2, the number of cells ($\times 10^6$), and non-dimensional simulation time.

2.2 Numerical methods and boundary conditions

The aerodynamic solver FUNk [27] used in this study, is based on the compressible Navier–Stokes equations expressed in conservative form. The spatial discretization method is based on the cell-centered Finite Volume methodology (FVM) on structured grid. An upwind biased scheme, with a third-order MUSCL interpolation scheme of AUSM+(P) family is used for the convective terms. A second-order-accurate centered scheme is used for viscous fluxes. The time integration is carried out by means of a third-order compact Runge–Kutta scheme. Two approaches are commonly used to perform LES with classical FV methods: explicit subgrid stress models are used to represent the effect of the unresolved scales of motion on the large scales and the second method consists in using the Monotonic Integrated Large-Eddy Simulations (MILES) proposed by Boris *et al.* [28]. The latter is based on the assumption that the intrinsic dissipation of an upwind scheme is able to mimic the dissipative behavior of the unresolved turbulent scales, and that when using such a scheme, no subgrid model is needed. This approach has been used in the present study.

At the entrance of the nozzle, uniform stagnation pressure, temperature profiles and velocity direction are imposed, thus, the boundary layers develop freely. Outside the nozzle, static pressure p_∞ = 101 325 Pa is imposed at the outflow boundary. On the lateral and upstream boundaries, non-reflecting boundary conditions are imposed using uniform external flow (static temperature T_∞ = 280 K and velocity U_∞ = 5 ms^{-1}). All the walls are assumed to be adiabatic. The time step of the Runge-Kutta scheme is $\Delta t = 2\times 10^{-8}$ s for Very Fine mesh (Fine: $\Delta t = 2\times 10^{-7}$ s).

The simulation is divided in two parts:

A first run (~ 100ms) is carried out to reach an established state for the turbulent jet mixing layer and for the acoustic field.

Then, the computation is performed for a physical time of about 100ms (500 D/U_j) for the aerodynamic and acoustic analyses. During this second run, time-averaged quantities are computed and instantaneous fields on the FW-H control surfaces are stored for acoustic analysis in far field. This time step storage for the FW-H calculations is small enough to correctly take into account the temporal scales of the acoustic phenomena.

Time histories of flow variables are also stored in the near field, on the jet axis, around the potential core end, and in the shear layer. Most of the signals are located inside the refined mesh zone. A common time step of $\Delta t_{sto} = 10^{-5}$ s (i.e., $\Delta t_{sto} \sim 0.05D/U_j$) has been used for all the storages.

2.3 Acoustic computation

The noise radiation is performed using the Ffowcs Williams and Hawkings surface formulation available in the code KIM [29] developed at ONERA. This formulation computes time pressure histories at any observer location by integration of the flow field solution on a control surface surrounding the jet and containing all the noise sources. For the Very Fine grid, two closed control surfaces extend over the entire length of the refined mesh zone, i.e., from X/D = -2 up to X/D = 25, while for the Fine mesh the same surfaces are not closed. These surfaces differ by their radial extent. The far field microphones are located at 75D from the nozzle exit for the directions between 20° and 150°, as in the experiments. Due to the spurious noise generated in aeroacoustics computations by the flow turbulence passing through a control surface, additional surface terms proposed by Rahier [30] are added in order to reduce this spurious noise. The results using different configurations of the control surface together with these additional surface terms is analyzed in the present paper.

3 AERODYNAMIC AND ACOUSTICS RESULTS

In this section, aerodynamic and acoustic results of the simulations with comparisons to measurements are presented and discussed in order to see how they reproduce the jet configuration. The mesh effects will be studied through the results comparison between both grid "Fine" and "Very Fine" with experimental data. First of all, the shear layer development and its initial state are studied. Then, the jet development is examined and how the near and far pressure fields match the experimental data.

3.1 Jet development

Figure 2 reproduces unsteady vorticity norm $|\omega|$ at the nozzle exit for both grids (left: Fine, right: Very Fine). It appears that, for the fine simulation, a part of the shear layer is laminar and exhibits pairings downstream of the nozzle exit. On the other hand, the transition from a laminar state to a turbulent state appears sooner for the Very Fine simulation (around X/D = 0.02) than for the other simulation (around X/D = 0.05). Moreover, the vorticity levels are higher in the Very Fine simulation, especially in the shear layer. As can be seen on axial vorticity snapshots in the plane Z/D=0 presented in Figure 3, the Very Fine simulation shows a vorticity field richer in small structures more tridimensional with more intense vortical structures than the Fine simulation. These results are confirmed by the snapshots of instantaneous axial vorticity for $-20\ U_j/D \leq \omega_x \leq 20 U_j/D$ in the three planes (from left to right) X/D=0.25, 0.5 and 1 for both meshes (top: Fine, bottom: Very Fine). Both simulations have similar vorticity field despite having different grid resolutions. An enlargement of the latter is given in Figure 4 in the plane X/D=0.25 for both meshes (left: Fine, right: Very Fine) and allows to understand the discrepancies between both simulations.

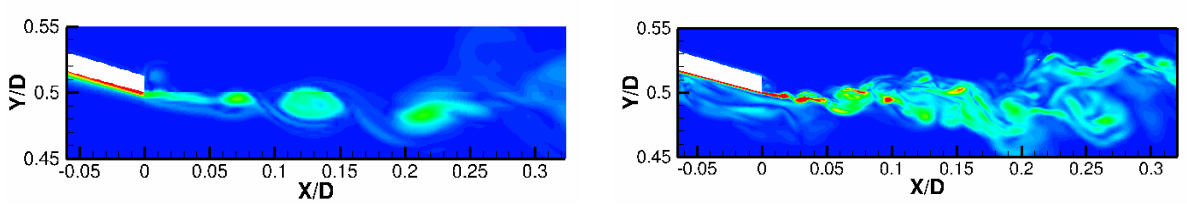

Figure 2: Instantaneous vorticity norm for $0 \leq |\omega| \leq 200Uj\ /D$ in the plane Z/D=0 downstream of the nozzle lip for both meshes (left: Fine, right: Very Fine).

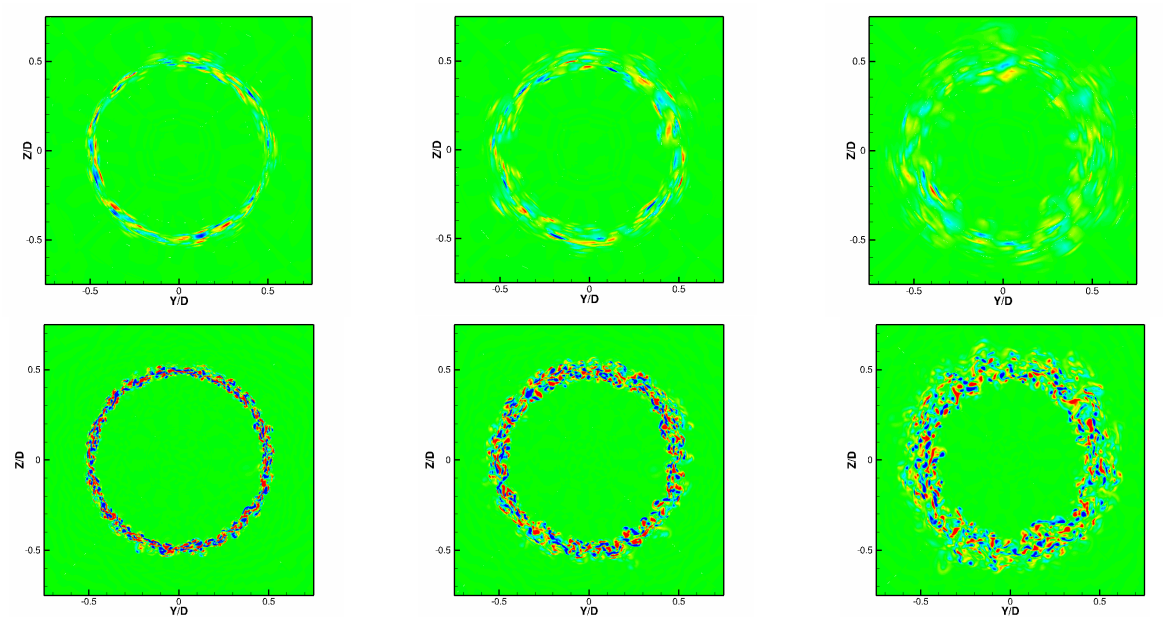

Figure 3: Instantaneous axial vorticity for $-20\ U_j\ /D \leq \omega_x \leq 20U_j\ /D$ in the three planes (from left to right) X/D=0.25, 0.5 and 1 for both meshes (top: Fine, bottom: Very Fine).

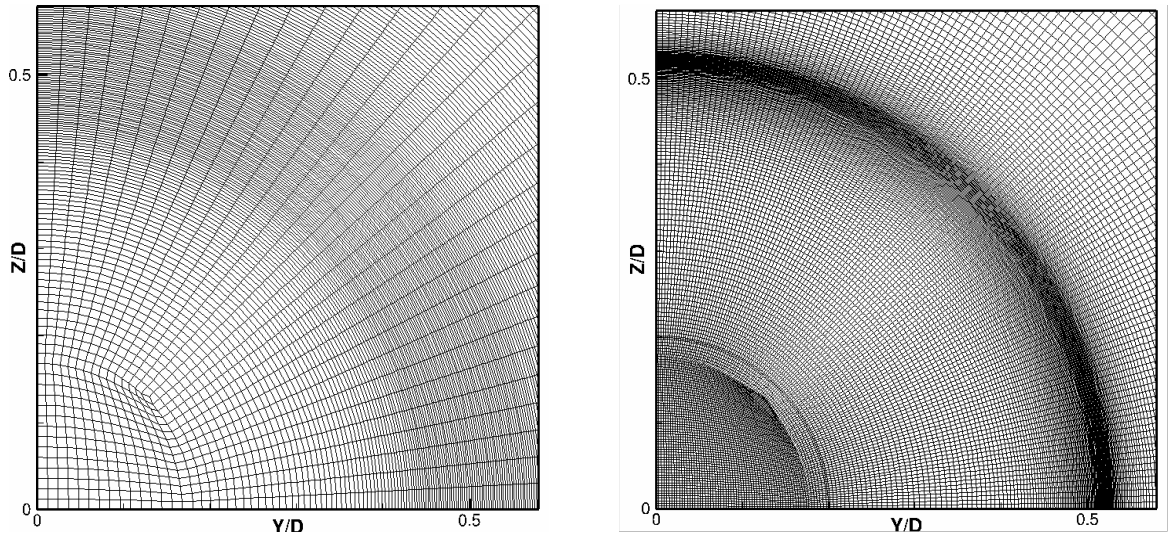

Figure 4: Enlargement of the grid in the plane X/D=0.25 for both meshes (left: Fine, right: Very Fine).

The shear layer state presented previously has an impact on the jet development. As can be seen in Figure 5, both simulations have different evolutions of the mean and rms axial velocity on the jet axis. The potential core $L_c\ /D$ corresponds to U_{mean}/U_j=0.95. Compared to experimental data, the Fine simulation has a shorter potential core length, around $L_c\ /D$ = 4.6,

while the Very Fine simulation has a larger one with L_c /D = 6.3. The axial location of the peak of rms for the Very Fine simulation is shifted downstream compared with the one obtained experimentally. Both simulations have a lowest peak of rms velocity compared to the experiments, due to the rms level (0.03) already present at X/D=0 in experimental measurements. The mesh refinement shows an impact on the rms peak location, but not on its level.

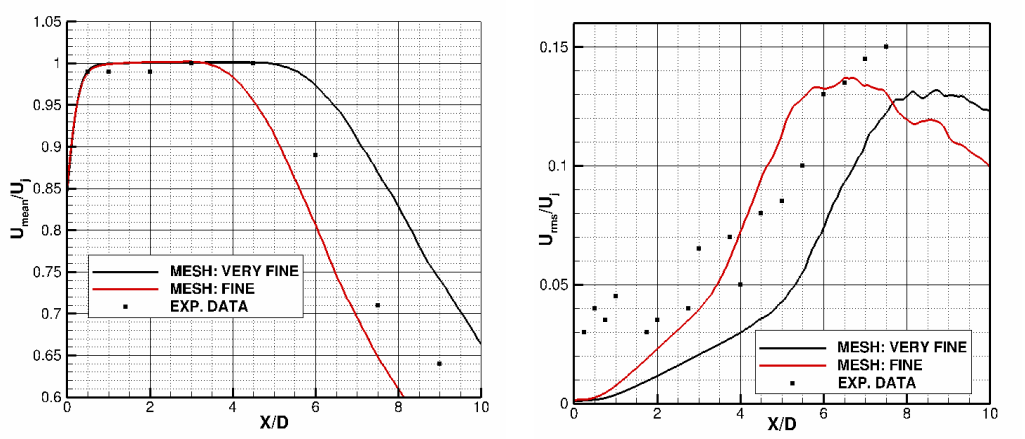

Figure 5: Comparison of the axial evolution on the jet axis of the mean and rms axial velocity for both simulations with experimental data.

Figure 6 shows rms values of the axial velocity normalized by the jet velocity as well as both control surfaces (S1, S2) for the Very Fine simulation. The highest levels of turbulence are located in the shear layers; they start at the vicinity of the nozzle exit and end downstream of the potential core, for X/D ≈ 10. This region of high turbulent fluctuations represents the major part of the acoustic sources, that radiate to the far-field. For axial positions downstream of X/D = 10, where U_{rms} /Uj = 13% close to the jet axis, the fluctuation level decreases with increasing axial distance. The turbulence level falls for instance to 5.5% of the jet velocity at X/D = 25 and to 4.1% at X/D = 30. An enlargement of U_{rms} /Uj in the vicinity of nozzle exit displayed in Figure 7 shows the flow laminarity at this location and confirms the beginning of turbulence around X/D = 0.02 found in the instantaneous vorticity field in Figure 2.

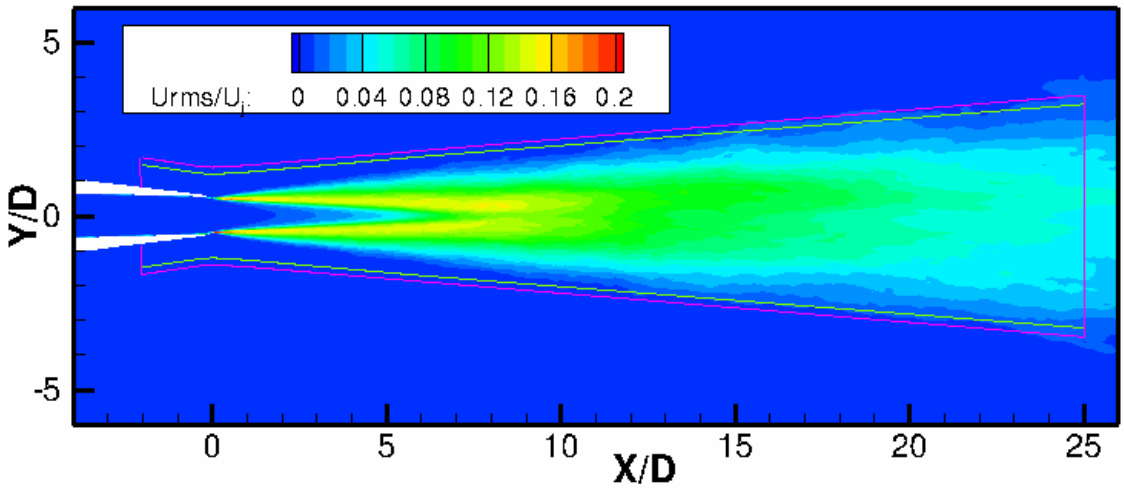

Figure 6: Iso-contours of rms axial velocity in the plane Z/D = 0 and integration surfaces (S1:blue and S2: purple) for acoustic calculations.

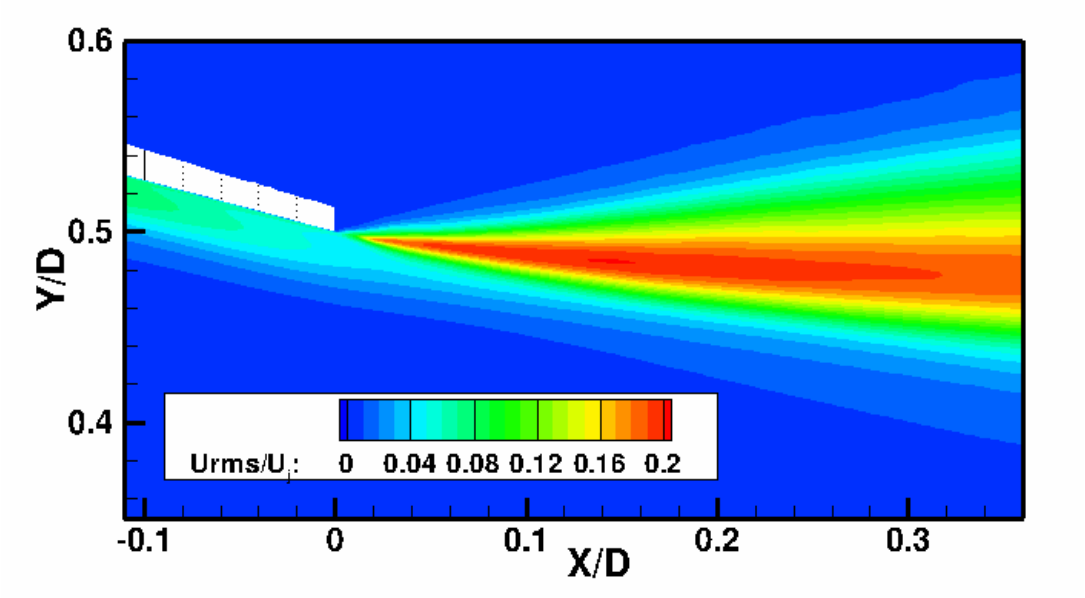

Figure 7: Iso-contours of rms axial velocity in the vicinity of nozzle exit.

3.2 Near field pressure

Thanks to pressure time histories stored in the near field, Figure 8 represents the axial evolution of the rms pressure levels, azimuthally averaged, at three different radial positions (r /D $\in$ {1.5; 3; 5}) for the Very Fine simulation and experimental data. For the three radial positions, a good agreement is observed between numerical and experimental data for X/D $\geqslant$ 4. However, for axial positions near the nozzle exit, an overestimation can be observed, especially for radial positions close to the jet (r/D = 1.5). At the location r/D=5, there is a good agreement between the experimental data and the simulation.

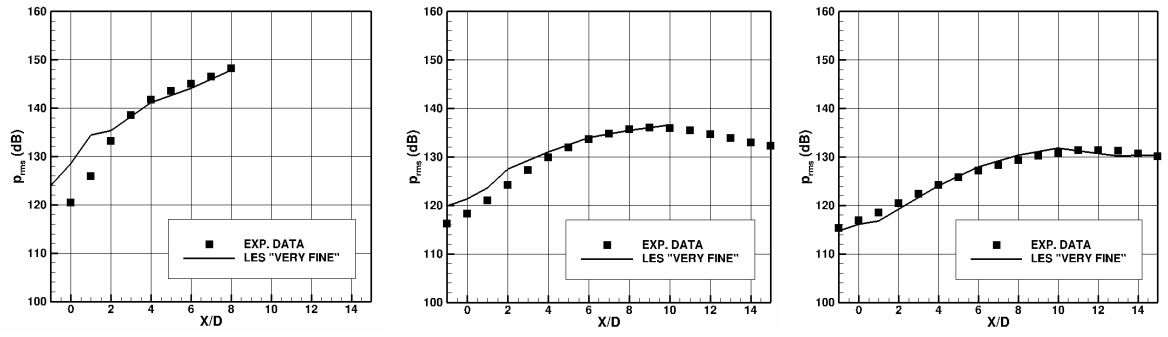

r/D=1.5 r/D=3 r/D=5

Figure 8: Comparison of the longitudinal evolution of the rms pressure at radial positions r /D $\in$ {1.5; 3; 5} between the Very Fine simulation and experimental data.

Hall *et al.* [31], Coiffet [32] and Muller [18] among other authors studied the azimuthal structure of near field pressure and observed that low wave number modes are dominant and the axisymmetric one (m=0) has a downstream growing contribution. The modes |m| < 5 include the most part of energy in the near field. The Strouhal number St is defined by St = f .D /U$_j$ where f corresponds to the frequency. The power spectral density (PSD) of the pressure signal of the axisymmetric mode are presented in Figure 9 for three different axial positions X/D=0, 4 and 8 and for two radial locations r/D=1.5 and 5. The overestimation observed for rms pressure levels at the location X/D=0 and r/D=1.5 is also visible on the power spectral

density (PSD) of the pressure signal for St $\in$ [0.4; 4]. A better agreement is observed when the axial distance is increased, which means that the sound radiated downstream is captured more accurately than the sideline radiated noise, because the turbulence fine scales require an higher mesh refinement. The effect of numerical dissipation on the PSD is also noticeable in Figure 9 at r/D = 5 for St $\geqslant$ 1. Apart from the overestimation visible for positions close to the nozzle exit, a good agreement between numerical and experimental data is found for axial positions X/D $\geqslant$ 4. The near field pressure is thus considered well reproduced by the simulation except for a zone around the nozzle exit.

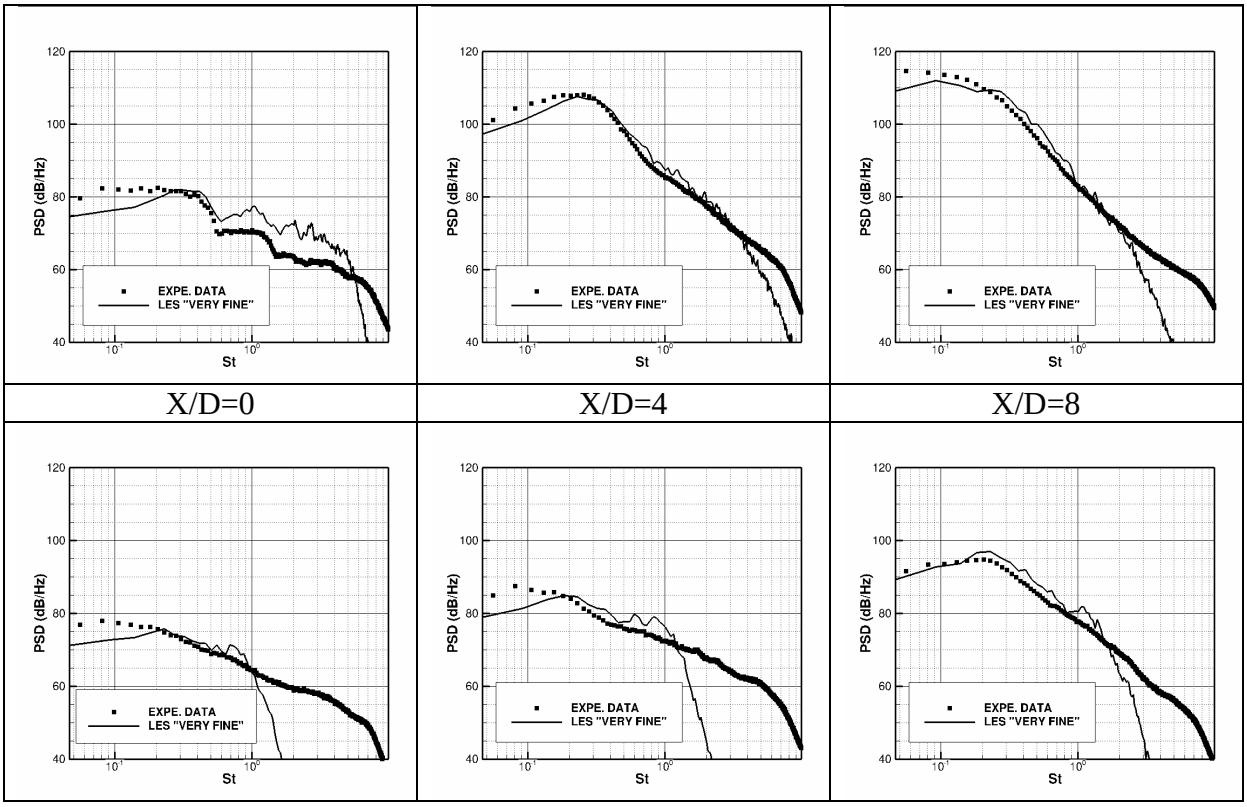

Figure 9: PSDs of the pressure field in the near field for different axial and radial positions : r /D = 1.5 (top), r /D = 5 (bottom) for m=0.

3.3 Far field pressure

The integration of the Ffowcs Williams and Hawkings (FW-H) equation on a porous surface allows determining the pressure radiated by a volume of perturbed fluid knowing the perturbation field on a closed control surface surrounding this volume. It is often used for noise prediction of isolated jets for which a control surface enclosing the mixing layer should contain all the noise sources. In theory, the control surface must be closed, but open surfaces can be used in practice if their extent is sufficiently large to enclose the noise sources adequately. However, if the control surface is closed, that reduces its extent and thereby the volume of data to be stored. In the present study, the FW-H method is used to analyze the acoustic content of the LES fields through the radiated pressure obtained in the far field. These radiation calculations are performed with two control surfaces S1 and S2 drawn in Figure 6, that axial and radial expanses are given below:

- Surface S1: from X_{min}/D = -2 to X_{max}/D = 25, r_{min}/D = 1.69, r_{max}/D = 4.52
- Surface S2: from X_{min}/D = -2 to X_{max}/D = 25, r_{min}/D = 1.98, r_{max}/D = 4.91

These surfaces are open for the "Fine" simulation and closed at X/D = -2 and X/D = 25 for the "Very Fine" simulation, but for this last case the surfaces can be analyzed open.

The signals obtained for a far field observation point, using the FW–H surface integral on the surfaces S1 and S2 open at both ends are compared in Figure 10. The predicted time histories are very similar and quite identical for both surfaces. This suggests firstly that the volume sources outside the control surface S1, not taken into account in the present acoustic analysis, make a very weak contribution to noise radiation. This result validates the choice of these control surfaces for the FW–H formulation. These similar signatures also demonstrate that the perturbation fields have been correctly transported from S1 to S2 by the aerodynamic calculation and therefore the CFD grid is sufficiently dense for a correct propagation of perturbations to the control surfaces. In the following analysis, only the surface S1 for "Very Fine" simulation is presented.

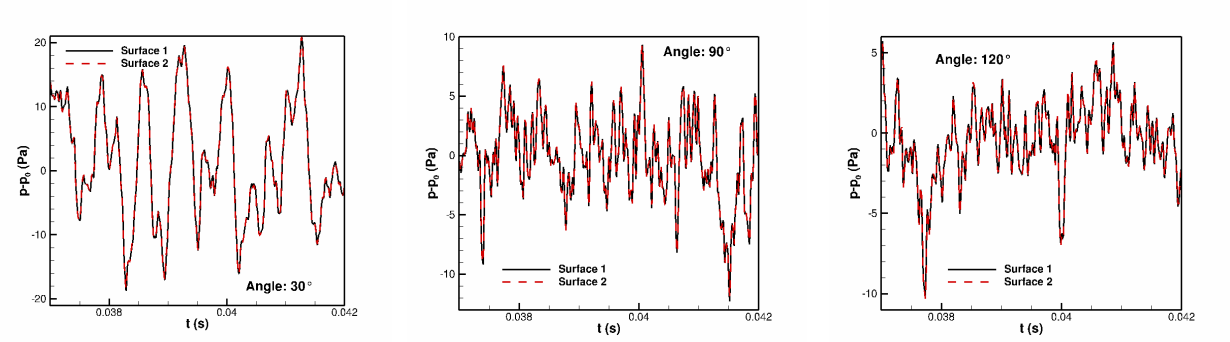

Figure 10: Time history of the pressure predicted in the far field (30°, 60° and 120°) using FW–H formulation on both integration surfaces for "Very Fine" simulation.

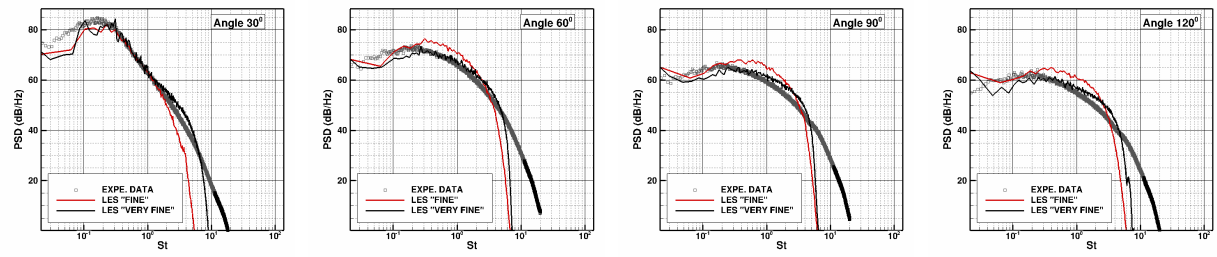

Figure 11 : Pressure Spectral Densities for four observer locations at r = 75D for both simulations compared to the experimental data.

The acoustic analysis is performed for 37 observation points uniformly distributed on a circle located in far field (75D from the nozzle exit) and centered on the nozzle exit, for comparison with experimental results. Their angular position θ is defined with respect to the jet axis and ranges from 0° (downstream) to 180° (upstream). The radiated pressures at the observer points are exploited only on 78 ms because of non reliable values in the beginning and in the end of the signals (incomplete contribution of the control surface because of the acoustic propagation delays). These radiated pressures are described also using a time step of 10^{-5} s. Fourier Transforms are applied on these signals and the levels are averaged over eight frequencies in order to smooth the spectra. These spectra are plotted for the range [0.2–20 kHz].

The comparison of the PSD between both simulations with open control surfaces and experimental data presented in Figure 11 for different angles 30, 60, 90 and 120° shows globally a better agreement for the Very fine simulation than for the Fine simulation with experimental

data. Underestimations are found for low frequencies St $\leqslant$ 0.1 and a slight overestimation for angles $\geqslant$90° for frequencies St $\geqslant$ 1.

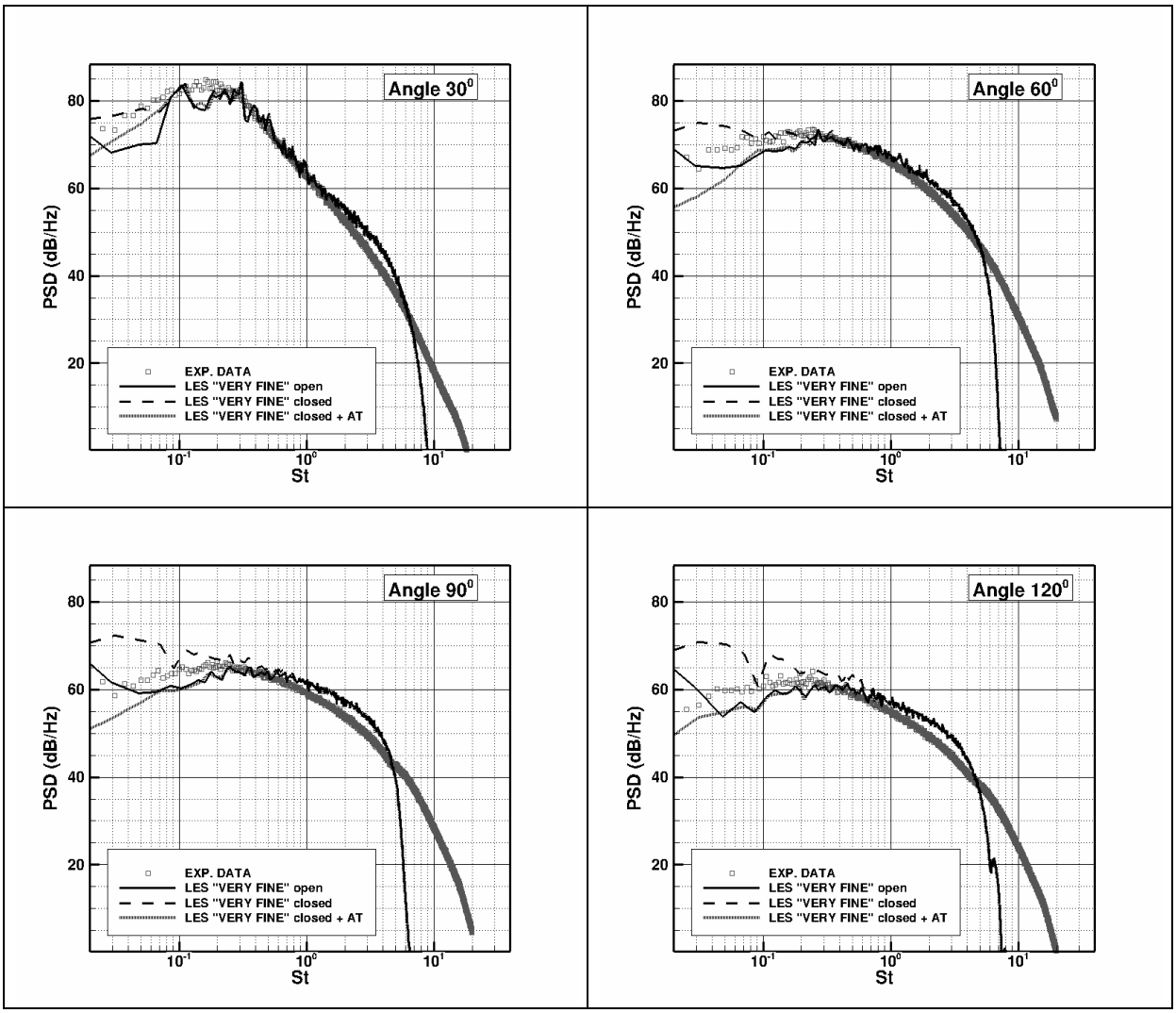

Figure 12: Pressure Spectral Densities for four observer locations at r = 75D for the Very Fine simulation (open, closed, closed + additional terms) compared to experimental data.

In [30], Rahier *et al.* proposed additional surface terms in order to reduce the spurious noise generated in aeroacoustic computations by the flow turbulence passing through a Ffowcs Williams and Hawkings (FW-H) control surface. This spurious noise is due to the fact that some volume sources are not taken into account in the calculations limited by surface integrations. An expression of additional surface terms representing an approximation of the missing volume integral has been defined. These additional terms include two separate Doppler amplification effects, respectively related to the flow velocity and to the control surface velocity and can be applied to any fixed or moving, rigid or deformable control surface. Compared to the use of open control surfaces, closed surfaces have the advantage of filtering any acoustic wave coming from the boundaries of the CFD grid. Another advantage for jet noise predictions is the ability to use shorter control surfaces that are less penalizing for the CFD grid refinement and for the storage of aerodynamic data for acoustic calculations. Short control surfaces have however the drawback of not taking correctly into account the refraction effects for the low angles of observation.

In the following, three configurations are tested and compared on the Very Fine simulation on the surface S1:

- LES Very Fine open : calculations without additional flux terms with the control surface S1 open at both ends.
- LES Very Fine closed : calculations without additional flux terms with the control surface S1 closed at both ends.
- LES Very Fine closed +AT : same as previously with additional flux terms.

Figure 12 presents the spectra comparison obtained for four observation angles, 30°, 60°, 90° and 120° for the three previous cases. Globally, for medium and high frequencies the PSD levels do not depend on the control surface and are in fairly good agreement with the experimental results. In contrast, at low frequencies the levels vary a lot with the control surface choice and appear to be largely overestimated for closed surface without additional terms. The more the angle is large, the more the overestimation concerns a wider band of frequencies. The stability of the results for the dominant frequencies of the actual acoustic radiation of the jet confirms that the main noise sources are contained inside the surface S1, because this surface extends very far downstream. It also confirms that open control surfaces commonly used for jet noise predictions can provide reliable results except for low frequencies.

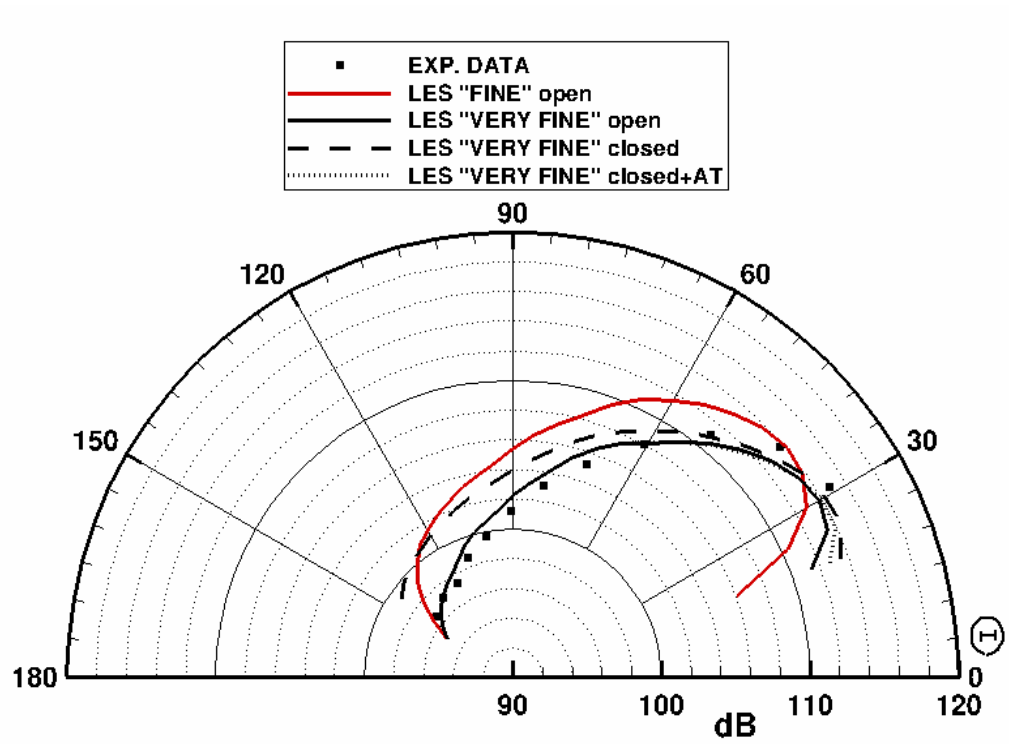

Figure 13: the overall sound pressure level (OASPL) directivity in the far field
for Fine and Very Fine (open, closed, closed +AT) simulations and experimental data.

The Overall Sound Pressure Levels (OASPL) for the directivities are calculated in the range [0.2–20 kHz] i.e. St $\in$ [0.4; 4] in accordance with the experimental data and presented in Figure 13. First of all, the comparison between Fine and Very Fine simulations with open surface shows clearly the improvement of the directivities due to the mesh refinement in all directions, especially in the azimuthal one, so as to obtain isotropic mesh cells with a grid cut-off frequency sufficiently high. The overall sound pressure level (OASPL) directivity in the far field is well predicted by the Very Fine simulation within a ±1 dB margin. However, overestimation due to pairings noise still remains, especially in the direction normal to the jet axis.

The acoustic directivities confirm that the use of closed control surfaces without additional flux terms is not suitable. Using closed control surfaces with additional flux terms seems to provide the same acoustic directivities as with an open control surface, because in this study this surface is long enough, except for low angles. Both acoustic directivity shapes are very close to the experimental data.

The overestimation for frequencies around St = 1, especially visible at 90◦ in the far field, is linked to the one observed in the near field for axial positions close to the nozzle exit (i.e., for X/D $\leqslant$ 4). Nevertheless, the difference is less visible in the far field. Indeed, at X/D = 0 and r/D = 1.5, there is an overestimation of around 6-7 dB/Hz, whereas for the signals in the far field at 90◦, the overestimation is about 4 dB/Hz. The high overestimation in the near field may be attributed to the hydrodynamic pressure, which amplitude decreases according to an exponential law, while the acoustic pressure amplitude decreases according to a $1/r^2$ law. The lower overestimation of 5 dB/Hz observed at X/D = 0 and r/D = 5 can be viewed as a consequence of the dissipation of the hydrodynamic part.

4 CONCLUSIONS

The present work deals with the numerical simulation of a hot subsonic turbulent jet using LES. The influence of the axial, radial, and azimuthal mesh refinements has been studied, thanks to a comparison between the present simulation (Very Fine) and a previous one (Fine) on the same jet configuration. The development of the shear layer depends on the mesh refinements. The vorticity field in the Very Fine simulation is richer in small structures and more tridimensional with more intense vortical structures than in the Fine one.

Despite having a good development, the shear layer remains laminar at the nozzle exit. Compared to the experimental data, the Fine simulation has a shorter potential core length, while the Very Fine simulation has a larger one. The axial location of the peak of rms for the Very Fine simulation is shifted downstream compared to the experimental one. At the nozzle exit, there is no turbulence in the jet center, so both simulations have a lowest rms velocity peak compared to the experiments.

The azimuthal structure of near field pressure confirms that axisymmetric one (m=0) has a downstream growing contribution. The overestimation observed for rms pressure levels at the location X/D=0 and r/D=1.5 is also visible on the power spectral density (PSD) of the pressure signal for St $\in$ [0.4; 4]. Due to the turbulence fine scales, that requires an higher mesh refinement, the sound radiated downstream is captured more accurately than the sideline radiated noise. For St $\geqslant$ 1 at r/D = 5, the numerical dissipation effect on the PSD is also noticeable. The near field pressure is thus considered well reproduced by the simulation except for a zone around the nozzle exit.

The Ffowcs Williams and Hawkings (FW-H) formulation is used for acoustic analysis of aerodynamic numerical simulations. This acoustic analysis is performed for observation points located in far field (75D from the nozzle exit) and centered on the nozzle exit for comparison with experimental results. Globally, the mesh refinement contributes to improve the Pressure Spectral Densities for different angles compared with experiments, although discrepancies are found for low frequencies (St $\leqslant$ 0.1) and for angles $\geqslant$90° for Strouhal St $\geqslant$ 1. Without additional flux terms, the turbulence passing through the downstream closing disk generates relatively high levels of spurious radiated pressure, which affects a wide band of frequencies, including the low frequencies. The use of closed control surface without additional flux terms has therefore no real interest for jet noise analysis. The results obtained using closed control surfaces with additional flux terms lead to the almost same results as the ones

obtained with open surface because the surface extent used in this study is long enough to include the main acoustic sources.

REFERENCES

[1] M. Wang, J. B. Freund, and S. K. Lele, Computational prediction of flow-generated sound, *Annual Review of Fluid Mechanics*, **38**, 483–512, 2006.

[2] J. B. Freund, Noise sources in a low-Reynolds-number turbulent jet at Mach 0.9, *Journal of Fluid Mechanics*, **438**, 277–305, 2001.

[3] X. Jiang, E. J. Avital, and K. H. Luo, Sound generation by vortex pairing in subsonic axisymmetric jets, *AIAA Journal*, **42**, 241–248, 2004.

[4] N. Andersson, L.-E. Eriksson, and L. Davidson, Large-eddy simulation of subsonic turbulent jets and their radiated sound, *AIAA Journal*, **43**, 1899–1912, 2005.

[5] D. J. Bodony, and S. K. Lele, On using large-eddy simulation for the prediction of noise from cold and heated turbulent jets, *Physics of Fluids*, **17**, 2005.

[6] C. Bogey, and C. Bailly, Computation of a high Reynolds number jet and its radiated noise using large eddy simulation based on explicit filtering, *Computers and fluids*, **35**, 1344–1358, 2006.

[7] S. R. Koh, W. Schröder, and M. Meinke, Turbulence and heat excited noise sources in single and coaxial jets, *Journal of Sound and Vibration*, **329**, 786–803, 2010.

[8] F. Vuillot, N. Lupoglazoff, and G. Rahier, Double-stream nozzles flow and noise computations and comparisons to experiments, *Proceedings of the 46th AIAA Aerospace Sciences Meeting*, No. AIAA 2008-9, 2008.

[9] K. B. M. Q. Zaman, Effect of Initial Condition on Subsonic Jet Noise, *AIAA Journal*, **23**, 1370–1373, 1985.

[10] M. Huet, Influence of boundary layers resolution on heated, subsonic, high Reynolds number jet flow and noise, *AIAA Paper*, 2013-2141, 2013.

[11] C. Bogey, O. Marsden, and C. Bailly, Influence of initial turbulence level on the flow and sound fields of a subsonic jet at a diameter-based Reynolds number of 10^5, *J. Fluid Mech.*, **701**, 352–385, 2012.

[12] C. Bogey, O. Marsden, and C. Bailly, Large-eddy simulation of the flow and acoustics fields of a Reynolds number 10^5 subsonic jet with tripped exit boundary layers, *Physics of Fluids*, **23**, 035104, 2011.

[13] K. B. M. Q. Zaman, Far-field noise of a subsonic jet under controlled excitation, *J. Fluid Mech.*, **152**, 83–111, 1985.

[14] C. K. W. Tam, Computational aeroacoustics: issues and methods, *AIAA Journal*, **33**, 1788–1796, 1995.

[15] C. K. W. Tam, Advances in numerical boundary conditions for computational aeroacoustics, *Journal of Computational Acoustics*, **6**, 377–402, 1998.

[16] L. S. Ukeiley and M. K. Ponton, On the near field pressure of transonic axisymmetric jet, *Int. J. Aeroacoustics*, **3**, 43–66, 2004.

[17] T. Suzuki and T. Colonius, Instability waves in a round jet detected using near-field phased microphone array, *J. Fluid Mech.*, **565**, 197–226, 2006.

[18] F. Muller, F. Vuillot, G. Rahier, and G. Casalis, Modal analysis of a subsonic hot jet LES with comparison to the linear stability, *Proceedings of the 11th AIAA/CEAS Aeroacoustics Conference*, No. AIAA 2005-2886, 2005.

[19] F. Muller, F. Vuillot, G. Rahier, G. Casalis, and E. Piot, Experimental and numerical investigation of the near field pressure of a high subsonic hot jet, *AIAA Paper* 2006-2535, 2006.

[20] B. Fayard, G. Rahier, and F. Vuillot, Modal analysis of jet flow from a coaxial nozzle with central plug, *AIAA Paper*, 2009-3355, 2009.

[21] J. W. Hall, J. T. Pinier, A. M. Hall, and M. N. Glauser, A spatio-temporal decomposition of the acoustic source in a Mach 0.85 jet, *AIAA Paper*, 2007-442, 2007.

[22] M. Lorteau, F. Cléro, and F. Vuillot, Analysis of noise radiation mechanisms in hot subsonic jet from a validated large eddy simulation solution, *Physics of Fluids*, **27**, 075108, 2015.

[23] J. E. Ffowcs Williams, and D. L Hawkings, Sound Generation by Turbulence and Surfaces in Arbitrary Motion, *Philosophical Transactions of the Royal Society of London*, **264**, A1151, 321-342, 1969.

[24] O. Piccin, CEPRA19: the ONERA large anechoic facility, *Proceedings of the 15th AIAA/CEAS Aeroacoustics Conference*, AIAA 2009-3303, 2009.

[25] O. Labbé, C. Peyret, G. Rahier, and M. Huet, A CFD/CAA coupling method applied to jet noise prediction. *Computers & Fluids*, **86,** 1-13, 2013.

[26] A. Biancherin, N. Lupoglazoff, F. Vuillot, and G. Rahier, Comprehensive 3D unsteady simulations of subsonic and supersonic hot jet flow-fields. Part 1: Acoustics analysis, *AIAA Paper*, 2002-2600, 2002.

[27] C. Laurent, I. Mary, V. Gleize, A. Lerat, and D. Arnal, DNS database of a transitional separation bubble on a flat plate and application to RANS modeling validation, *Computers & Fluids*, **61**, 21-30, 2012.

[28] J. P. Boris, F. F. Grinstein, E. S. Oran, R. L. Kolbe, New insights into large eddy simulation. *Fluid Dyn Res*,**10**,199–228, 1992.

[29] G. Rahier, J. Prieur, F. Vuillot, N. Lupoglazoff, and A. Biancherin, Investigation of integral surface formulations for acoustic post-processing of unsteady aerodynamic jet simulations, *Aerosp. Sci. Technol.*, **8**, 453–467, 2004.

[30] G. Rahier, M. Huet, J. Prieur, Additional terms for the use of Ffowcs Williams and Hawkings surface integrals in turbulent flows, *Computers & Fluids* **120,** 158-172, 2015.

[31] J. W. Hall, J. T. Pinier, A. M. Hall, and M. N. Glauser, A spatio-temporal decomposition of acoustic source in a Mach 0.85 jet, AIAA paper, **442**, 2007.

[32] F. Coiffet, P. Jordan, J. Delville, Y. Gervais, F. Ricaud, Coherent structures in subsonic jets : a quasi-irrotational source mechanism? *International Journal of Aeroacoustics*, Multi-Science Publishing, 2007.